地 震 研 究 所 彙 報
Bull. Earthq. Res. Inst.
Univ. Tokyo
Vol. 81 (2006) pp. 55-70

Contemporary Stress Field in the Wadati-Benioff Zone at the Japan-Kurile Arc-arc Junction (North Honshu, the Hokkaido Corner and Hokkaido Island) by Inversion of Earthquake Focal Mechanisms

Cenka Christova[1,2)]*, Naoshi Hirata[2)] and Aitaro Kato[2)]

[1)] Geophysical Institute of Bulgarian Academy of Sciences, Dept. of Seismology, Acad. G. Bonchev str. Bl 3, Sofia 1113, Bulgaria

[2)] Earthquake Research Institute, the University of Tokyo 1-1-1 Yayoi Bunkyo Tokyo 113-0032, Japan

Abstract

This study addresses the space distribution of the stress field in the Wadati-Benioff zone of Northeastern Japan and southernmost Kurile area based on homogeneous data of earthquake focal mechanisms and the inverse technique by Gephart and Forsyth (1984). The data set used consists of 785 JMA focal mechanism solutions (FMS) and 97 FMS listed in Kosuga *et al.* (1996) for shallow and intermediate depth earthquakes. The detailed analysis of the space distribution of orientation of P (compression) and T (extension) axes of FMS allowed the outlining of the following WBZ subvolumes for which we applied the stress inversion: three planar structures in North Honshu (NH) and the Hokkaido corner (HC) WBZ (Plane1, Plane 2, Plane 3), and upper and lower subvolumes in the Hokkaido Island (HI) WBZ. The stress field parameters are evaluated along the northeastern Japan and southern Kurile arcs for these WBZ subvolumes.

The stress field in Plane 1, mainly low-angle thrust faults, is characterized by shallow dipping and close to strike normal maximum compression $\sigma 1$ and down dipping minimum compression $\sigma 3$. Plane 2, the upper surface of the WBZ below 60～70 km in NH and HC, is under slab parallel $\sigma 1$ and close to slab normal $\sigma 3$ all along NH, while in HC the minimum compression rotates counterclockwise about 30° relative to the slab normal. Plane 3, the lower surface of the WBZ, is characterized by close to slab normal $\sigma 1$ and close to slab parallel $\sigma 3$. The stress regime in Plane 1 is of general compression everywhere but in segment HT, beneath the Hokkaido corner, where it is of general extension (Guiraud, 1989). The stress regime in Plane 2 is of general compression, and in Plane 3- of pure extension.

A characteristic feature of the two WBZ subvolumes outlined beneath Hokkaido is that the upper subvolume overlies the lower one everywhere but in the southern part of the island. The orientations of the maximum and minimum compressive stresses in the upper subvolume of the Hokkaido WBZ, considered relatively to the local slab geometry, are similar to these in Plane 1 of NH and HC WBZ, i.e. close to strike normal $\sigma 1$ and down dipping $\sigma 3$. However, the dip of the principle stresses is different - here $\sigma 1$ is steeper and $\sigma 3$ is shallower. The stress field in the lower WBZ subvolume beneath Hokkaido is characterized by strike aligned $\sigma 3$ dipping north at about 50°, $\sigma 1$ trends SE being strike normal beneath the southern part of the island and slab normal beneath its northern part. The orientations of P and T in the upper WBZ subvolume in central Hokkaido differ significantly from these in the upper WBZ volumes to the south and to the north but are similar to those in the lower subvolume here. The stress inversion results indicate homogeneous stress field in the upper and lower WBZ subvolumes beneath central Hokkaido. The orientation of the minimum compression here (strike aligned, trending north) is close to the orientations of $\sigma 3$ in the southern

* e-mail : cenka@.geophys.bas.bg (Geophysical Institute of Bulgarian Academy of Sciences, Dept. of Seismology, Acad. G. Bonchev str. Bl 3, Sofia 1113, Bulgaria)

and northern lower parts of the HI WBZ, while the $\sigma 1$ is dipping steeply WSW. These stress directions, if considered kinematically, indicate that the preferred faulting occurs at plane that is almost vertical and perpendicular to the strike of the slab (the strike of the trench) with the northern wall moving down and the southern one moving up. The stress regime is of general extension in all the considered subvolumes in the HI WBZ.

The results of this study clearly indicate 3-planar distribution of stresses in the WBZ beneath North Honshu and the Hokkaido corner. We outlined two subvolumes (upper and lower) in the WBZ beneath Hokkaido, which are characterized by different orientations of the principle stresses. The stress field in the upper WBZ subvolume is perturbed by a deformation zone (DZ), located beneath central Hokkaido. This DZ is perpendicular to the slab's strike and is cutting through the slab, the stresses in the upper and lower subvolumes of it are of similar orientation. The directions of the best-fit stress model in the DZ suggest that its northern wall moves down while its southern wall moves up. One plausible explanation is that this deformation zone represents a crack or a tear cutting through the entire slab.

Key words: Wadati-Benioff zone, North Honshu- Kurile junction, regional stress field, inverse method

1. Introduction

The Japan-Kurile arc-arc junction, roughly limited by the latitudes 38°-46°N and the longitudes 138°-148°E includes North Honshu, the Hokkaido corner and Hokkaido Island located on the North American or the Okhotsk microplate plate (e.g. Takahashi *et al.,* 1999). The bathymetric map and the main structural units of the study area are presented in Fig. 1. The estimates of the convergence rate between the North American and the Pacific plates indicate that it is of about 9 cm/yr (e.g., DeMets *et al.,* 1994). Here the active subduction of the Pacific plate results in a well-defined but of complicated geometry Wadati-Benioff zone (WBZ) (e.g., Sasatani, 1976; Stauder and Mualchin, 1976; Hasegawa *et al.,* 1978; Moriya, 1978; Suzuki *et al.,* 1983). According to these studies, the dip of the subducting Pacific plate changes significantly from 25°–30°, beneath North Honshu to 40°–45° beneath the central and northern Hokkaido. The change in the dip of the slab results in a slab folding, the location of which is shown by the shaded area A1 in Fig. 2 (see also Fig. 3 in Moriya, 1978). Recently Katsumata *et al.* (2003) studied the geometry of the WBZ at the Japan-Kurile arc-arc junction, based on earthquake hypocenters relocated by a dense local seismic network and 3-D P and S velocity structures. Their model suggests that the dip of the subducting slab changes from 20°–30° beneath the Japan arc to 40°–50° beneath Southern Kuriles. The increase of the slab dip is observed in a

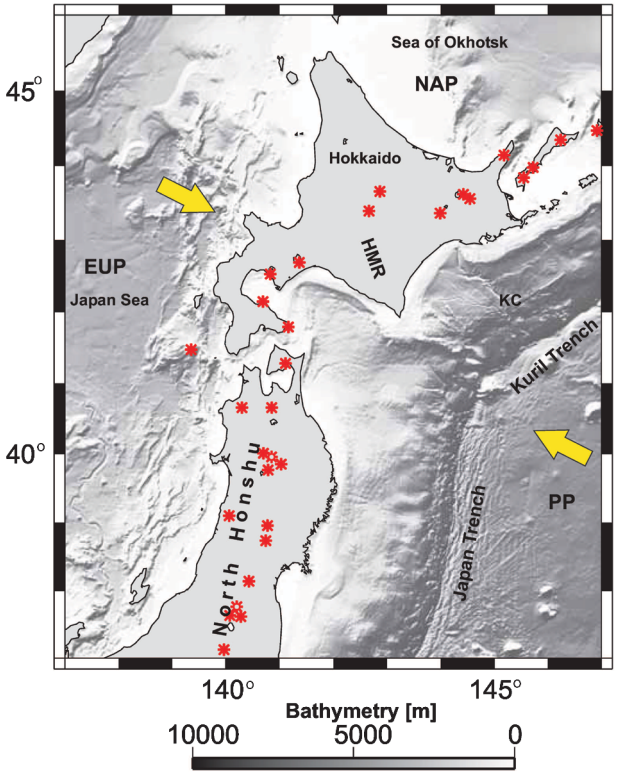

Fig. 1. Bathimetric map and main structural units of the study area. Arrows show the direction of convergence of the lithospheric plates (DeMets *et al.,* 1994). The main structural units are denoted as follows: NAP-North American plate, PP-Pacific plate, EUP Euroasian plate, HMR-Hidaka Mountain Range, KC-Kushiro Canyon. The active volcanoes (JMA, 2005) are marked by open stars.

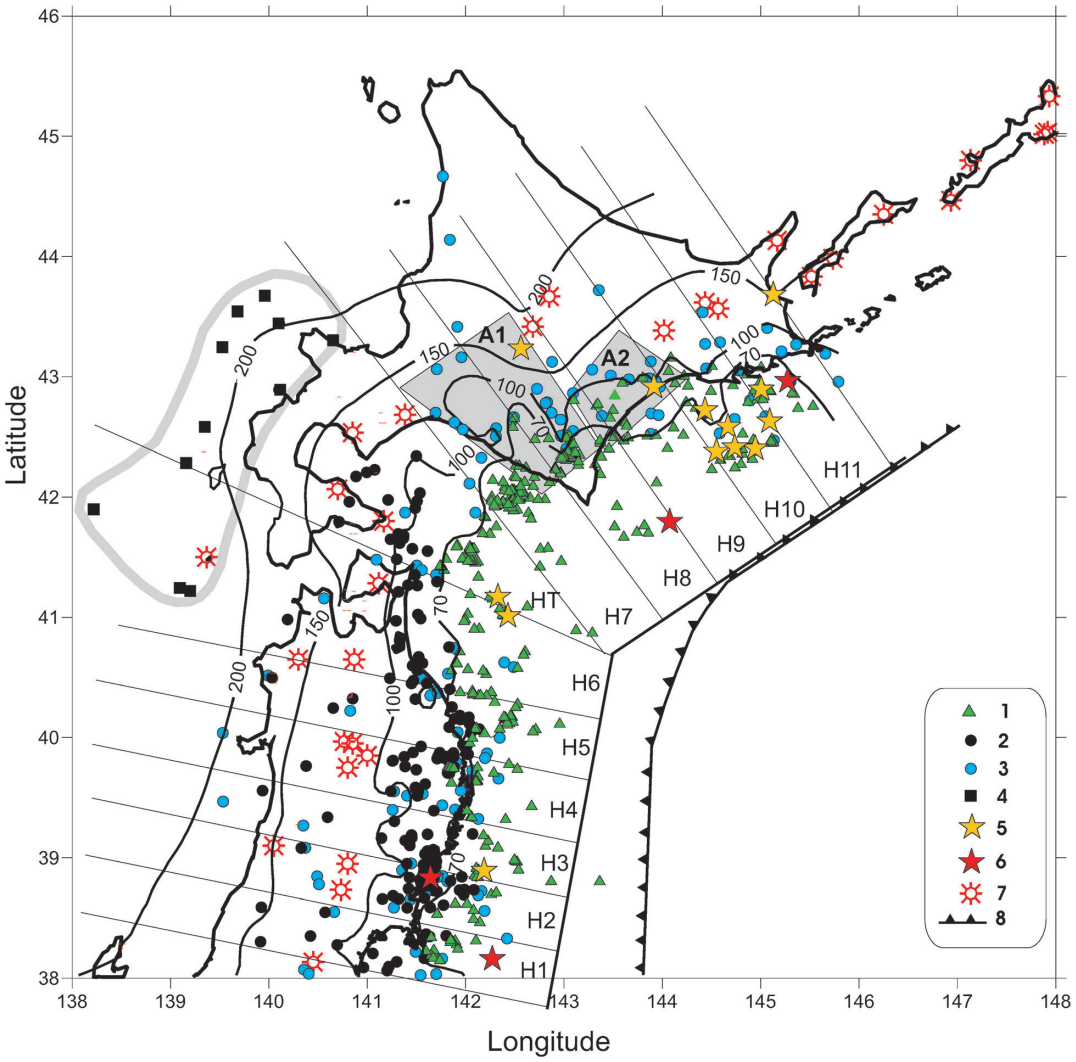

Fig. 2. Epicenter map of earthquakes with available focal mechanisms used for determining the stress field parameters in the Wadati-Benioff zone beneath North Honshu, Hokkaido corner and Hokkaido Island. The epicenters are marked by different symbols depending on the subvolumes of the WBZ they belong to: 1-Plane 1, shallow low-angle thrust events, in North Honshu and the Hokkaido corner, and the upper WBZ subvolume beneath Hokkaido; 2-Plane 2, the upper surface of the WBZ, 3-Plane 3, the lower surface of the WBZ, in North Honshu and the Hokkaido corner, and the lower WBZ subvolume beneath Hokkaido; 4-the deep earthquakes in North Honshu and the Hokkaido corner; 5-earthquakes of magnitude in the range $6.0 \leq Md \leq 6.9$; 6-earthquakes of magnitude in the range $7.0 \leq Md \leq 8.0$; 7-active volcanoes; 8-trench axis. The solid lines are the contours of 70 km, 100 km, 150 km and 200 km hypocentral depth and show the dip trend of the WBZ. The position of the deep seated earthquakes is outlined by a thick gray contour. The gray area A1 depicts the location of the slab folding according to Morya (1978); the gray area A2 marks the location of the transition zone where the dip of the slab steepens rapidly according to Katsumata *et al.* (2003).

narrow transition area depicted in Fig. 2 by the shaded area A2. The authors found an unusual distribution of microearthquakes within the Pacific plate, which was located on a near-vertical plane striking perpendicular to the Kurile trench. Katsumata *et al.* (2003) named this feature the Tokachi-Oki slab-cracking zone and suggested that it is a slab-cracking zone torn by the extensional stress due to the rapid lateral changes in the dip of the subduction zone. The rapid change of the dip of the slab in the above area was confirmed recently by detailed P and S wave tomography and space distribution of seismicity (Miller *et al.*, 2006).

Previous studies on stresses in the study area were based on analysis of earthquake focal mechanisms (FMS) or composite FMS for small and micro-

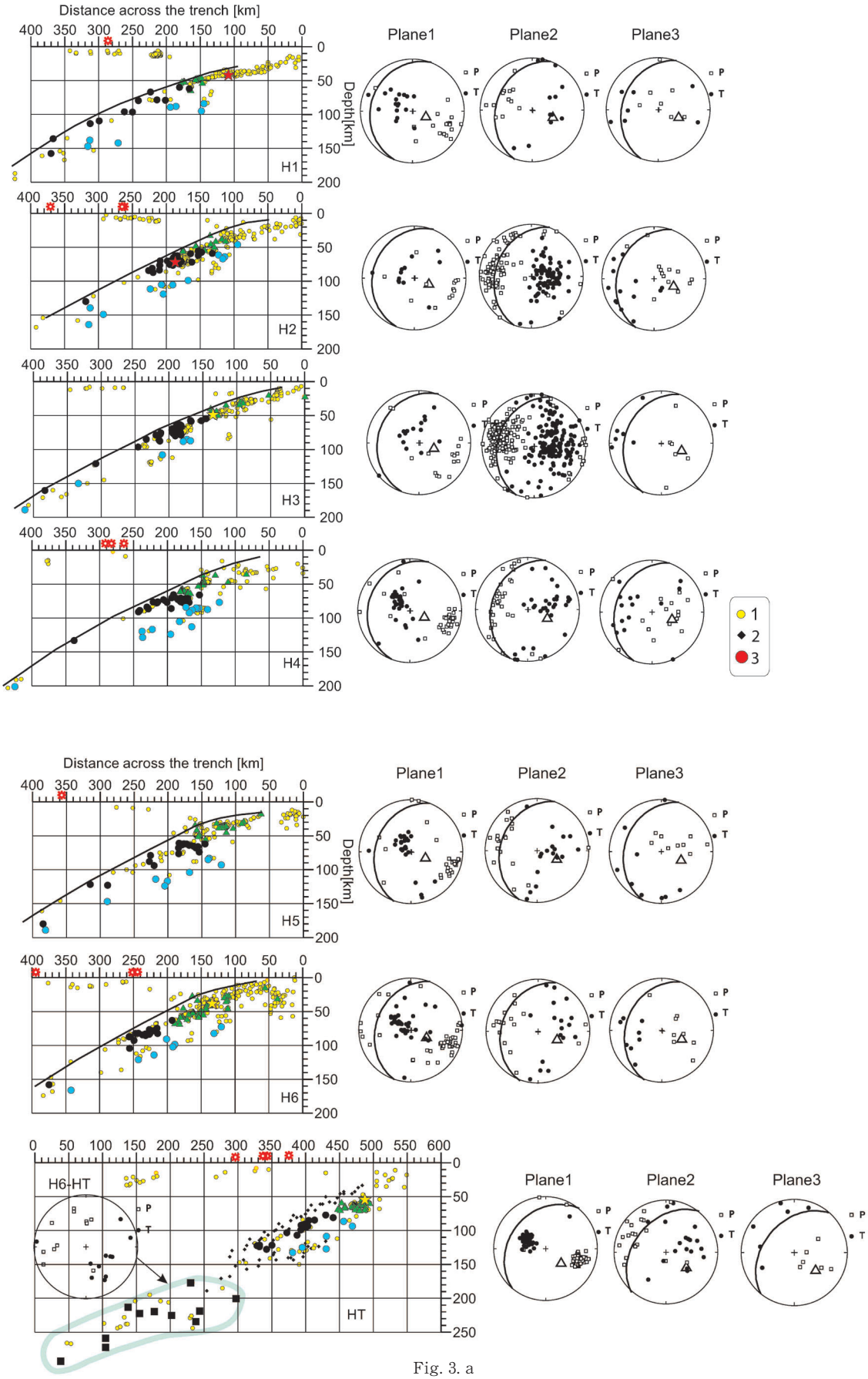
Distance across the trench [km]
Depth [km]
Plane1
Plane2
Plane3
H1
H2
H3
H4
H5
H6
H6+HT
HT
P
T
1
2
3

Fig. 3. a

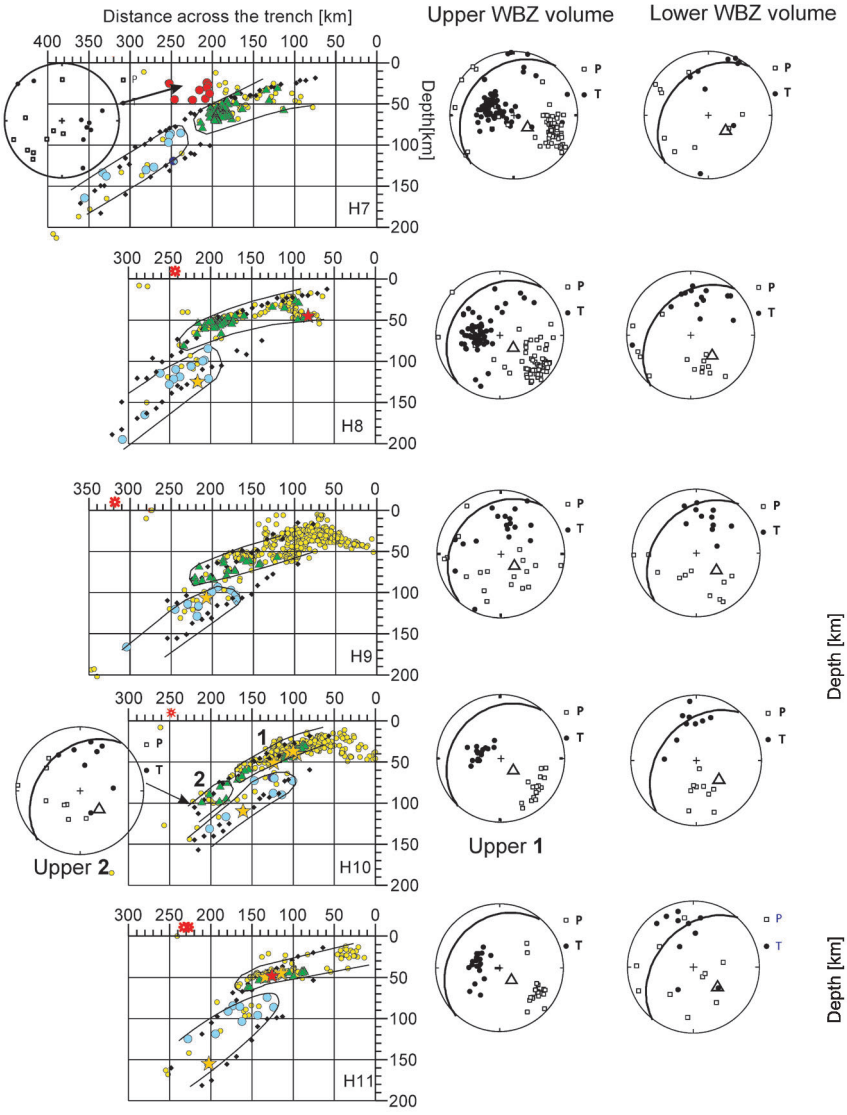

Fig. 3. b

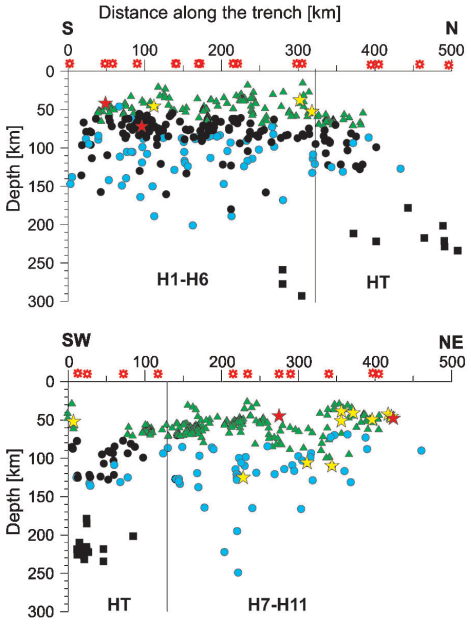

Fig. 3. c

Fig. 3. Depth distribution of the considered earthquake foci and the overall seismicity (JMA seismological bulletin of Japan for the period 2002–2006) to true scale relatively to the trench axis (vertical scale=horizontal scale): (a) across the trench in North Honshu and the Hokkaido corner; note that Plane 1 overlies Plane 2 with segment H6 being an exception; (b) in the Hokkaido area; (c) along the trench, here the earthquakes depth distribution in the Hokkaido corner is shown together with the North Honshu seismicity (at the top) and with the seismicity beneath the Hokkaido area (at the bottom). The symbols for the earthquake hypocenters as in Figure 1, the additional symbols used are as follows: heavy line for the upper surface in the WBZ; 1-the JMA hypocenters of overall seicmicity; 2-limits of the upper and lower surface of the WBZ according to Katsumata *et al.* (2003); 3-hypocenters of earthquakes forming a fractured zone in the continental plate overlying the WBZ in the Hokkaido area. The orientations of the P (small open squares) and T (solid circles) axes of the earthquake focal mechanisms, the subducting plate (heavy curve) and its normal (empty triangle) are projected onto lower hemisphere equal-area plots for each WBZ subvolume.

earthquakes (e.g. Isaks and Molnar, 1971; Umino and Hasegawa, 1975; Sasatani, 1976; Stauder and Mualchin, 1976; Yoshii 1979; Suzuki *et al.,* 1983; Kosuga *et al.,* 1996). It was found that the WBZ beneath North Honshu and the Hokkaido corner has two-planar structure with predominant down dip extension in the upper plane and down dip compression in the lower one (e.g., Umino and Hasegawa, 1975; Hasegawa *et al.,* 1978; Hasegawa *et al.,* 1983; Umino *et al.,* 1984; Kosuga *et al.,* 1996). Seno and Pongsawat (1981)

found out that the WBZ off Miyagi Prefecture in North Honshu has a 3-planar structure that consists of a shallow thrust zone and the so-called double-planed seismic zone. The low-angle thrust zone overlaps the double-planed seismic zone. Recently, Igarashi *et al.* (2001) have shown that the 3-planar seismic structure is continuously distributed throughout northeastern Japan. Based on analysis of 33 FMS of intermediate depth earthquakes located on the upper surface of the HI WBZ, Katsumata *et al.* (2003) outlined a transition zone beneath central Hokkaido where the orientations of the T axes range from ENE-WSW to NNW-SSE and indicate for extensional stress regime. They explain this stress regime as due to the rapid lateral changes in the dip of the subducting slab.

Although the analyses of the orientation of the P and T axes from earthquake FMS give information about the stress field and deformations in a given area, still two ambiguities remain: the identification of the primary fault plane and the auxiliary plane, and the relation of the P and T axes with the maximum and minimum principal compressive stress directions. To distinguish between the two fault planes a comparison with the local geology is usually used but this approach cannot be applied in the present case because intermediate depth earthquakes are considered here. The use of the P and T axes for determining the directions of maximum and minimum compressive stresses is correct only if the stress drop tensor is equivalent to the stress tensor. However, because of preexisting zones of weakness slip can occur in a variety of orientations relative to the principal stresses, i.e. a fault plane, which coincides with a zone of weakness, may bear no unique geometric relation to the stress directions (McKenzie, 1969). Inverse techniques for solving the regional stress tensor from earthquake focal mechanisms have been developed to overcome the above problems (e.g., Gephart and Forsyth, 1984; Michael, 1984; Angelier, 1998).

Recent studies on stress field in several Wadati-Benioff zones carried out by stress inversion of FMS have shown that this approach gives new and more quantitative information about regional stress field and thus about the subduction dynamics in the studied regions (e.g., Cacamo *et al.,* 1996; Christova 2001, 2004, 2005; Christova and Nikolova, 1998; Christova and Scholz, 2003). Christova and Tsapanos (2000) studied the depth distribution of stresses in the Hokkaido WBZ by stress inversion of Harvard CMT solutions. According to them, at depth below 60 km, along strike extension trending N-NE and compression of orientation varying from ESE to SW are involved in the subduction dynamics. These results indicate that the slab pull and the mantle resistance, acting on the slab edge, are not the only forces that control the contemporary plate tectonics in the Hokkaido region.

Our study focuses on evaluating the spatial distribution of contemporary stress field in the WBZ in Northeast Japan and southernmost Kuriles based on the use of homogeneous earthquake focal mechanism data (the Japan Meteorological Agency Annual Seismological Bulletin of Japan, JMA) and the inverse technique of Gephart and Forsyth (1984) in attempt to obtain further insights about the stress field and stress regime in the WBZ beneath North Honshu, the Hokkaido corner and the Hokkaido Island.

2. Inverse method for determining the stress tensor

The inverse method by Gephart and Forsyth (1984) (GF84) is used herein for evaluating the stress field parameters in the Wadati-Benioff zone beneath North Honshu, the Hokkaido corner and Hokkaido Island. The inverse technique GF84 allows for determining the directions of the principal stresses $\sigma1$, $\sigma2$, $\sigma3$ ($\sigma1 \geq \sigma2 \geq \sigma3$) and the ratio $R=(\sigma2-\sigma1)/(\sigma3-\sigma1)$ ($0 \leq R \leq 1$). The value of R estimates the magnitude of the intermediate principal stress ($\sigma2$) relative to the maximum ($\sigma1$) and the minimum ($\sigma3$) principal stresses. The R value, combined with the spatial orientations of the principal stresses relatively to the slab geometry (slab plane and its normal), gives also information about the stress regime in the WBZ. We use here the stress regime classification as defined by Guiraud *et al.* (1989).

Basic assumptions in the GF84 method are: (1) the stress tensor is uniform in the space and time considered; (2) earthquakes are shear dislocations and can occur on pre-existing faults, and (3) slip occurs in the direction of the resolved shear stress on the fault plane. The algorithm searches for the stress tensor showing the best agreement with the avail-

able earthquake focal mechanisms by minimizing the sum of the misfits. For a given stress model, the misfit of a single focal mechanism is defined as the smallest rotation about any arbitrary axis that brings the slip direction and sense of slip of either of the two nodal planes into an orientation that is consistent with the stress model. The confidence limits of the solution are computed by a statistical method (Parker and McNutt, 1980; Gephart and Forsyth, 1984). When performing the stress inversion one of the maximum or minimum principal stresses is chosen as a primary stress and the other - as a secondary one.

The value of the average misfit θ corresponding to the best stress model provides a guide as to how well the assumption of stress homogeneity is fulfilled, i.e. the GF84 method can be used to investigate possible stress heterogeneity in a volume or during earthquake sequences by analyzing subsets of the data population (Gephart and Forsyth, 1984).

Because it is supposed that the value of the average misfit θ is composed of contributions from errors in the P and T orientations and heterogeneity in the tectonic stress field, additional criteria should be used for checking the fulfillment or breakdown of the assumption of homogeneous stress field in a considered area. The errors in the data used, the value of the average misfit, and the 95% confidence range are usually used for this purpose (e.g. Gephart and Forsyth, 1984; Gillard *et al.,* 1996; Lu *et al.,* 1997). The discrepancy in the orientation of P and T axes reported by different catalogues, e.g. Harvard, USGS and ERI, is estimated to be less than 15° (Helfrich, 1997; Frohlich and Davis, 1999). Here the value of 15° was accepted as a realistic uncertainty in the P and T axes orientations of our data sets. The assumption of stress homogeneity in each volume can be checked in the light of results from tests carried out by Gillard *et al.* (1996), and Lu *et al.* (1997). According to them, small and moderate errors (5°–15°) that could realistically be expected in a data set of focal mechanisms cannot lead to average misfits larger than 6°, thus $\theta < 6°$ and well constrained stress directions (the 95% confidence regions of $\sigma 1$ and $\sigma 3$ do not overlap) suggest a homogeneous stress field. When the stress directions are not well constrained and the average misfit is larger than 10°, it is attributed to stress heterogeneity; and when θ is in the range $6° < \theta < 10°$ the solution reflects some heterogeneity of the stress field (Gillard *et al.,* 1996; Lu *et al.,* 1997).

3. Data, data analysis and outlining of WBZ subvolumes

963 earthquake focal mechanism data from the JMA Annual Seismological Bulletin of Japan for the period 1997-March 2006 and 127 focal mechanisms for the period 1986-1990 listed in Kosuga *et al.* (1996) were analyzed for the purposes of the present study. In total, we found 882 focal mechanisms for intermediate depth events that occurred in the WBZ of the

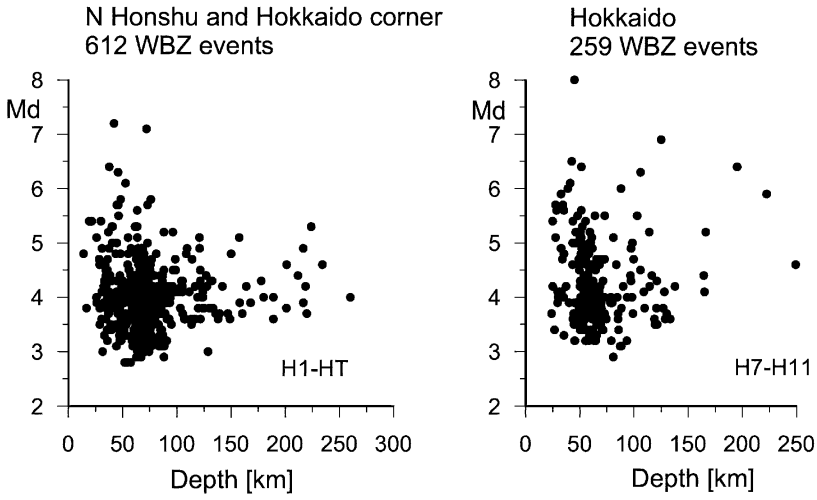

Fig. 4. Depth distribution of the displacement magnitue (Md) of the earthquakes, with available focal mechanisms used in the stress inversions, which belong to the Pacific plate subducting beneath North Honshu and the Hokkaido corner, and beneath Hokkaido Island.

study area. The epicentral map of the selected earthquakes is shown in Fig. 2. Different symbols are used for representing earthquakes which belong to the different WBZ subvolumes defined and outlined by a procedure described below.

1) First the geometry of the WBZ was delineated based on space distribution of the overall seismicity (JMA, 2002–2006) and the upper and lower WBZ surfaces outlined by Katsumata *et al.* (2003). For this purpose, we constructed 12 cross sections perpendicular to the trench axis showing the depth distribution of overall seismicity relatively to the trench, and then we delineated the geometry of the WBZ along the arc as a slab-like body (see Fig. 2a, b). The cross sections are 6 for North Honshu, one triangular section (HT) for the Japan-Kurile arc-arc junction, and 5 for Hokkaido Island, (see Fig.2 and 3 a, b). The width of these sections is about 60 km. For the Hokkaido corner (note that here we refer the triangular section HT to the Hokkaido corner) and Hokkaido (H7-H11) we used the limits of the upper and lower surface of the WBZ listed in Katsumata *et al.* (2003) as additional control for outlining the WBZ geometry. Because the upper surface of the WBZ in segments HT (see Fig 2a) and H7-H11 is well defined by Katsumata *et al.* (2003) it is not indicated by a heavy line in Fig. 2b.

2) The earthquakes with available JMA FMS (963 events) for the period 1997- March 2006 were plotted on the depth sections and of them 785 earthquakes that belong to the subducting Pacific Plate were identified.

3) We added 97 FMS for WBZ earthquakes that occurred in the period 1986–1990 listed in Kosuga *et al.* (1996).

4) Based on analysis of the space distribution of orientations of the P and T axes of the individual earthquake focal mechanisms and the local geometry of the slab, we outlined the following WBZ subvolumes characterized by a predominant type of FMS: three planar structures beneath NH and HC, and upper and lower subvolumes beneath Hokkaido. The outlined WBZ subvolumes, the orientations of the corresponding P and T axes with respect to the local strike and dip of the slab (lower hemisphere equal area projections) are shown fore each cross section in Fig. 3 (a, b). The depth distribution of the selected earthquake foci along the Japan and Kurile trenches is shown in Fig. 3c. Because the strike of trench changes at the Japan-Kurile arc-arc junction in the area of HT segment, the earthquakes depth distribution in it is shown together with the North Honshu seismicity (at the top) and with the seismicity beneath the Hokkaido area (at the bottom).

We are aware of the fact that the above procedure cannot ensure complete elimination of the plate interface earthquakes, especially in the shallower part of Plane 1 beneath NH and HC, but the stress field in it is also analyzed because the FMS of these events also provide information about the subduction dynamics.

The magnitude Md of the selected earthquakes (Md- displacement magnitude, JMA Annual Seismological Bulletin of Japan, 1997) is in the range 2.9–8.0, the distribution M versus depth (h) is shown in Fig. 4. Most of the selected earthquakes are of magnitude larger than 3.0.

Because both the orientations of the principal stresses in the slab reference frame (the slab plane and its normal) and the R value are used for determining the stress regime in the WBZ, we follow the classification of the orientations according to previous studies of stresses in Wadati-Benioff zones by stress inversion of FMS (e.g., Christova and Tsapanos, 2000; Christova 2001, 2004, 2005; Christova and Scholz, 2003): slab parallel - dipping in the direction of the slab being parallel to the slab's plane, down-dip - dipping in the direction of the slab's dip but steeper than the slab; slab normal - close to the perpendicular to the slab plane; strike normal - close to the perpendicular to the strike of the slab (i.e. to the trench axis); along strike - close to parallel to the strike of the slab; in slab - lying in the plane of the slab.

The prevailing orientations of the P and T axes relatively to the local geometry of the slab, i.e. its dip, strike and normal, in the outlined WBZ subvolumes are described below.

In the WBZ of North Honshu (segments H1-H6 and HT):

Plane 1: mainly low angle thrust events with down dip T and close to strike normal P axes, the depth penetration of this plane is about 60–70 km and it overlies Plane 2.

Plane 2: in slab P axes clustering in a direction parallel to the dip of the slab, and T axes in a plane that is

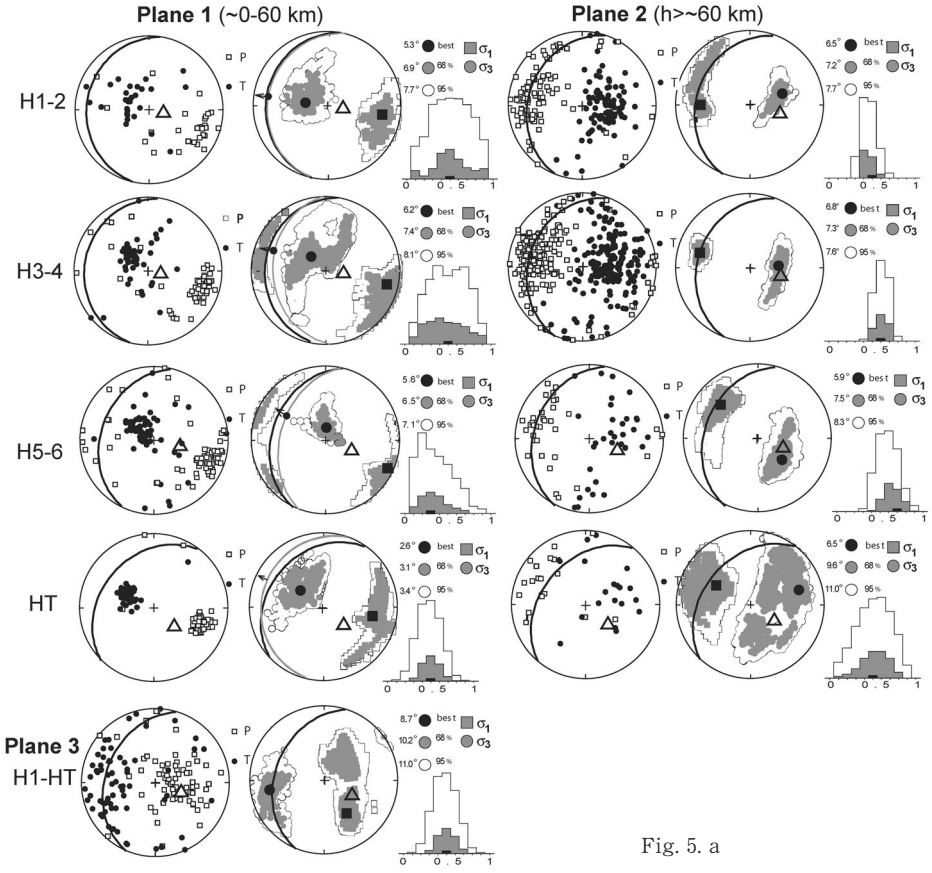

Fig. 5. a

normal to the slab but clustering around the slab normal.

Plane 3: in slab T and P that cluster around the slab normal.

In the WBZ of Hokkaido:

Upper WBZ subvolume: close to down dip T and close to strike normal P. This subvolume overlies the lower one everywhere beneath Hokkaido but in segment H7, its depth penetration is about 90 km being shallowest in segment H11 (～70 km).

Lower WBZ subvolume: the T axes are of NW to NE orientation with a tendency to cluster toward North, the P axes are scattered in the southern hemisphere.

Note that for NH and HC WBZ we use the term 'plane' instead of 'subvolume' because here the earthquake hypocenters with available FMS form planar structures.

Two additional groups of earthquakes with available FMS were found, but because the number of the data for them is rather small the stress inversion did not give reliable solutions. The first group is located in segments H6 and HT and consists of 11 earthquakes of depth in the range 170–300 km (see Figures 2, 3a, 3c). The P and T axes of this group trend NW and SE, respectively. The second group is located in segment H7 in the continental wedge and consists of 9 earthquakes (see Fig. 2b). The FMS of these earthquakes show some clustering of P axes in the SW quadrant, while the T axes are mostly in the SE quadrant.

Based on the above analysis the GF84 inversion was applied along the arcs for Planes 1 and 2 in segments H1–H6, we consider Plane 3 as a whole over segments H1–HT, and for the upper and lower subvolumes in H7–H11. We combine neighbour segments along the trench for subvolumes where the stress inversion gives similar orientations of the principal stresses, or where the number of FMS is insufficient for reliable stress inversion. Different weights were given to the stress inversion input data depending on the earthquake magnitude: 1 for $2.9 \leqq Md \leqq 5.9$; 2 for $6.0 \leqq Md \leqq 6.4$; 3 for $6.5 \leqq Md \leqq 7.0$; 4 for $7.1 \leqq Md \leqq 8.0$.

4. Results of the stress inversion

We first performed a coarse initial grid search

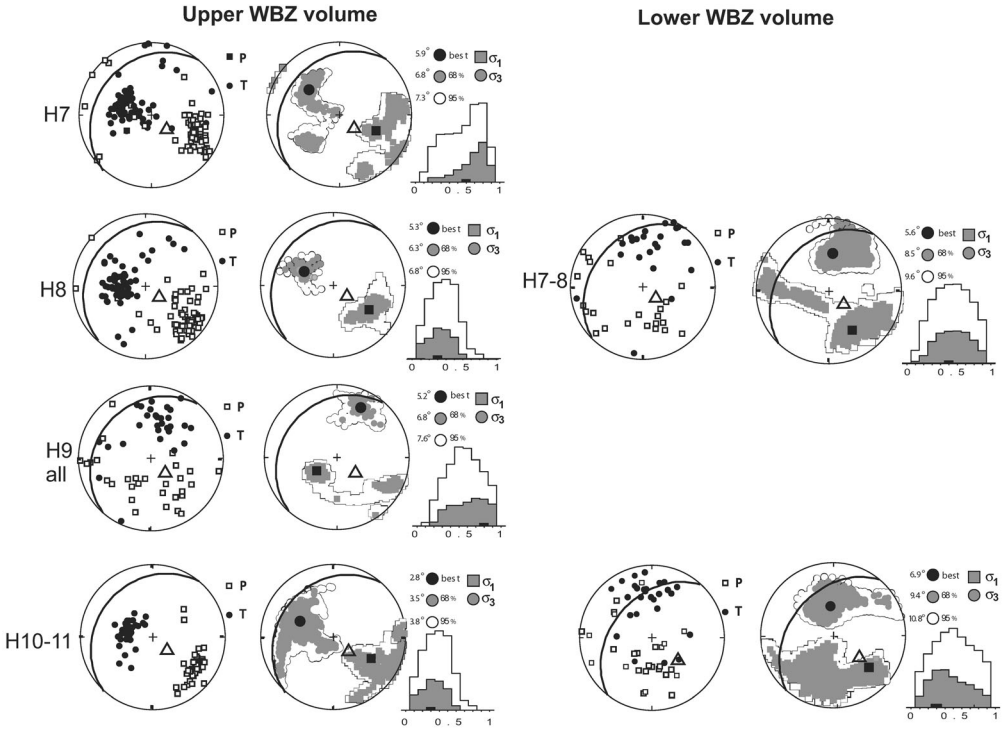

Fig. 5. b

Fig. 5. Depth distribution of the directions of principal stresses the Wadati-Benioff zone as determined by the stress orientation inversion: (a) beneath North Honshu and the Hokkaido corner; (b) beneath Hokkaido Island. The WBZ subvolumes are shown at top, the segments' index on the left; the left column depicts the orientations of P and T axes (small open squares and solid circles, respectively) of the focal mechanisms of each data set; the right column shows the directions of the corresponding best-fit maximum $\sigma 1$ and minimum $\sigma 3$ compressive stresses (large solid squares and circles, respectively), as well as their 68% and 95% confidence ranges. The histograms show the distribution of the number of tested stress models within the 68% and 95% confidence ranges relative to the stress ratio R, the best-fitting stress model is indicated by black. The projection of the subducting slab and its normal are denoted by a heavy curve and an empty triangle, respectively. The primary fault planes of the best-fit stress models obtained for Plane 1 in North Honshu WBZ are depicted by thin gray curves, also shown the slip vectors for the primary fault planes. All directions are projected onto lower hemisphere equal-area plot.

(10° spacing in stress orientations) covering the whole range of possible stress models for each data set by the approximate method FMSIA (Gephart and Forsyth, 1984). We then perform the exact method FMSIE (Gephart and Forsyth, 1984) with the results of the FMSIA as starting models and a fine grid search (5° spacing in stress orientations) over 45° and 90° cones around the primary and secondary principal stresses, respectively. The whole range of possible stress models were covered by FMSIE considering each $\sigma 1$ and $\sigma 3$ as a primary stress. The best-fit stress solutions, and their 95% and 68% confidence limits obtained by the inversion for the NH, HC and HI WBZ are presented as lower hemisphere projections in Figs. 5a and 5b respectively. Table 1 and Table 2 list the local dip of the slab to NW, the number of the input data, and the best-fit stress models obtained for the considered WBZ subvolumes: the directions of $\sigma 1$, $\sigma 2$, $\sigma 3$, the R value estimate, and the average misfit θ.

The main features in the depth distribution of the P and T data and the stress field parameters in the outlined subvolumes of the Wadati-Benioff zone beneath NH, the HC and HI, as inferred from the stress inversion, are described below.

For each subvolume considered we analyzed the orientations of the P and T axes, and the estimated directions of the maximum ($\sigma 1$) and minimum ($\sigma 3$) principal stresses with respect to the slab reference frame.

Table 1. Results for the best fit stress models in segments H1-H6 and HT. N-number of earthquake focal mechanisms used in the inversion; σ1-maximum compressive stress; σ2-intermediate compressive stress; σ3-minimum compressive stress; $R=(\sigma2-\sigma1)/(\sigma3-\sigma1)$ magnitude ratio of principal stresses (see text); θ-average misfit angle. All searches are in cones of 90° for the primary and secondary stress; the grid is 5°.

Depth range [km] Segment	Dip of the slab	N	σ_1 dip/azimuth	σ_2 dip/azimuth	σ_3 dip/azimuth	R	θ- misfit [°]
0~60 **Plane 1**							
H1-2	20°	30	25°/100°	2°/9°	65°/275°	0.5	5.3
H3-4	20°	50	18°/103°	10°/196°	69°/314°	0.6	6.2
H5-6	30°	66	1°/115°	9°/205°	81°/20°	0.3	5.6
HT	30°	53	30°/103°	3°/194°	60°/290°	0.4	2.6
h>~60, **Plane 2** (Upper plane)							
H1-2	30°	102	35°/268°	8°/173°	54°/72°	0.5	6.5
H3-4	30°	193	34°/288°	8°/192°	55°/90°	0.6	6.8
H5-6	30°	35	34°/313°	0°/222°	56°/132°	0.7	5.9
HT	40°	19	48°/300°	24°/180°	32°/74°	0.5	6.5
Plane 3 (Lower plane)							
H1-6 and HT	30°~40°	64	44°/144°	35°/ 9°	25°/260°	0.5	8.7

Table 2. Results for the best fit stress models in segments H7-H11. N-number of earthquake focal mechanisms used in the inversion; σ1-maximum compressive stress; σ2-intermediate compressive stress; σ3-minimum compressive stress; $R=(\sigma2-\sigma1)/(\sigma3-\sigma1)$ magnitude ratio of principal stresses (see text); θ-average misfit angle. All searches are in cones of 90° for the primary and secondary stress; the grid is 5°.

Segment	Dip of the slab	N	σ_1 dip/azimuth	σ_2 dip/azimuth	σ_3 dip/azimuth	R	θ- misfit [°]
Upper WBZ volume							
H7	25°	77	44°/114°	13°/216°	43°/318°	0.7	5.9
H8	25°	61	30°/129°	8°/32°	50°/292°	0.4	5.3
H9-all	25°-30°	29	68°/222°	7°/113°	20°/20°	0.8	5.2
H10-11	25°	40	39°/126°	14°/20°	48°/279°	0.3	2.8
Lower WBZ volume							
H7-8	30°	25	37°/155°	15°/257°	49°/5°	0.5	5.6
H10-11 1st model	40°	27	33°/136°	19°/239°	50°/354°	0.3	6.9
2nd model			28°/221°	26°/111°	50°/350°	0.7	7.2

North Honshu and Hokkaido corner

Plane1

The data in Plane 1 show P axes that are shallow dipping to ESE being close to normal to the strike of the slab. The T axes toward NW being steeper than the plane of the slab, i.e. down dip (Fig. 5a, Table 1). The stress inversion results reflect these orientations, showing well defined shallow dipping to ESE and close to strike normal σ1 and down dip minimum compression σ3, its dip being about 40°–60° steeper than the dip of the slab. A characteristic feature is that the principle stresses in segment HT have the same orientations as in segments H1-H6 but here their dip is different: σ1 is steeper thus being close to slab normal, while σ3 is shallower. The stress directions are well resolved in terms of the 95% confidence limits and the value of the misfit thus indicating homogeneous stresses in the considered segments. According to the classification by Guiraud *et al.* (1989), close to slab normal σ3, in slab σ2 and σ1, and values of R ranging from 0 to 1, indicate a stress regime of general compression. The directions of the minimum and maximum compression in Plane 1 along segments H1-H6 deviate from these orienta-

tions but the components of $\sigma 3$ and $\sigma 1$ in the slab reference frame (the slab plane and the slab normal) are significant thus indicating that the prevailing stress regime in Plane 1 of the WBZ beneath North Honshu is of general compression. The stress inversion result for segment HT, the Hokkaido corner, shows close to slab normal $\sigma 1$ while both $\sigma 3$ and $\sigma 2$ are in the slab plane, the value of R is 0.4. This suggests that the stress regime in Plane 1 is of general extension (Guiraud *et al.,* 1989).

The outlined here Plane 1 represents a thin layer forming the upper surface of the WBZ to depth about 60 km and thus it includes mainly earthquakes, which are traditionally considered as interplate earthquakes. Therefore we also give the kinematic presentation of the stress inversion results for Plane 1 - the preferred (primary) fault planes and slip vectors for the obtained best-fit stress tensors (see Fig. 5 a). Fig. 5 a shows that the primary fault planes almost coincide with the slab everywhere and the slip vectors are slab parallel as it should be expected. An exception is the solution for HC (segment HT) where the preferred fault plane and the corresponding slip vector are rotated at about 30° counterclockwise relatively to the slab plane and slab parallel direction, respectively.

Plane 2

The data pattern in Plane 2 is more scattered in respect to those in Plane 1 (Fig. 5a). The P axes cluster in slab parallel direction but show a greater range of directions from down dip to along the slab strike. The T axes cluster in slab normal direction, but show a greater range of directions in a plane normal to the slab. The T axes in segment HT rotate counterclockwise in respect to the slab normal. The stress inversions show slab parallel $\sigma 1$ and close to slab normal $\sigma 3$ in segments H1-H6, while in segment HT $\sigma 3$ rotates at about 30° counterclockwise in respect to the slab normal (Fig. 5a, Table 1). However this rotation is not significant in terms of 95% confidence limits. The stress directions are well resolved in terms of the 95% confidence limits but the values of misfit are slightly greater than 6.0° thus indicating for possible small stress heterogeneities. The obtained close to slab normal $\sigma 3$, and in slab $\sigma 2$ and $\sigma 1$ directions in Plane 2 and the R values indicate that stress regime here is of general compression (Guiraud *et al.,* 1989).

Plane 3

The T axes are in the slab plane, and cluster in slab parallel direction showing a greater range of directions along the slab strike. The P axes cluster in slab normal direction. The stress inversion result shows close to slab normal $\sigma 1$ and close to slab parallel $\sigma 3$ (Fig 5a, Table 1). The stress directions are well resolved in terms of the 95% confidence limits, the estimate of the misfit is 8.7 and indicates possible heterogeneity in the stresses in lower plane of the WBZ. The obtained close to slab normal $\sigma 1$, and in slab $\sigma 2$ and $\sigma 3$ directions and $R=0.5$ indicate that stress regime in Plane 3 is of pure extension (Guiraud *et al.,* 1989).

Hokkaido

Upper WBZ volume

The data in the upper WBZ subvolume show P axes that are shallow dipping to SE being close to normal to the strike of the slab. The T axes toward NW being steeper than the plane of the slab, i.e. down dip (Fig. 5b). The stress inversion results reflect these orientations. The orientations of the maximum and minimum compressive stresses, considered relatively to the local slab geometry, are similar to these in Plane1 of NH and HC WBZ, i.e. close to strike normal $\sigma 1$ and down dipping $\sigma 3$. (Fig 5b, Table 2). However, the dip of the principle stresses is different -here $\sigma 1$ is steeper and $\sigma 3$ is shallower. The earthquake foci in the upper WBZ subvolume of segment H10 show a spatial clustering in two groups (see Fig. 3b). The orientations of P and T axes of group 1 are similar to these in the upper WBZ subvolumes in segments H7, H8 and H11. Group 2 has P and T of orientations similar to the lower WBZ subvolume and we include this group of earthquakes in the data set for the lower WBZ subvolume.

We found out a specific feature in the upper WBZ subvolume. The orientations of P and T in central Hokkaido (segment H9) differ significantly from these in the upper WBZ volumes to the south and to the north of it, but are similar to the P and T orientations in the lower subvolume here. The stress inversion results indicate homogeneous stress field in upper and lower WBZ subvolumes beneath central Hokkaido if these subvolumes are considered together. The orientation of the minimum compression here (strike aligned, trending north) is close to the orientations of $\sigma 3$ in the southern and northern

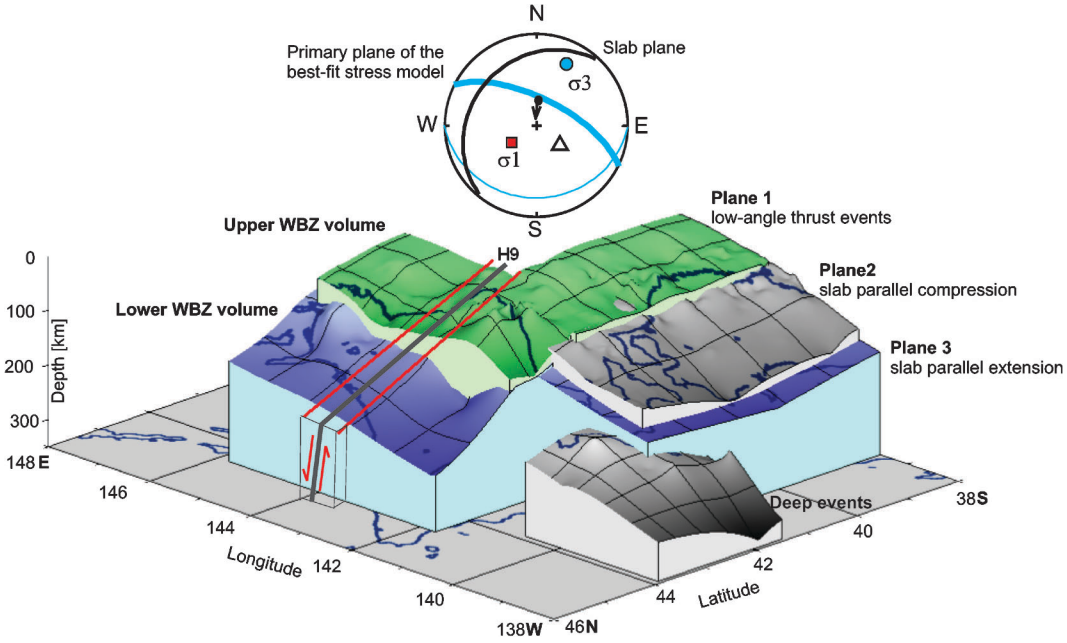

Fig. 6. 3-D orthogaphic representation (view from NW) of the geometry of the outlined Wadati-Benioff subvolumes for which we evaluated the stress field parameters. The surfaces are constructed based on the earthquake hypocenters data (events used in the stress inversions) that belong to the individual subvolumes. The colors used for the surfaces of the WBZ subvolumes are as for the earthquakes in Figures 2 and 3. The position of segment H9 is marked by red lines. The plane of the suggested tear fault (the primary fault plane from the best-fit stress model) that cuts through the slab in H9 is marked by thick blue line, red arrows indicate the slip on it-the northern wall moves down, the southern one-up. Above the scheme are shown the orientations of the principle stress direction of the best-fit stress model obtained for segment H9: red for $\sigma 1$, blue for $\sigma 3$, the curved lines are the projections of the slab plane (black), the primary (thick blue), and auxiliary (thin blue) planes of the best-fit stress model, also shown the slip vector for the primary fault plane; the slab normal indicated by triangle. All projections are onto lower hemisphere.

lower parts of the Hokkaido WBZ, while the $\sigma 1$ is dipping steeply to WSW. These results indicate that the area of H9 represents a deformation zone (DZ), which cuts through the subducting slab and the stress orientations in it differ significantly from the stresses in the whole upper WBZ subvolume. The stress regime in the upper WBZ subvolume beneath Hokkaido is of general extension (Guiraud *et al.*, 1989). The position of segment H9 can be seen in 3-D view in Fig. 6 where it is marked by red lines. Figure 6 summarizes the outlined herein geometry of subvolumes in the Wadati-Benioff zone. The shown surfaces are constructed based on the earthquake hypocenters data (events used in the stress inversions) that belong to the individual WBZ subvolumes. The scheme shows the plane of the suggested possible tear of the slab, and the movement of its walls. The low hemisphere projection shown above this scheme depicts the orientations of the principle stresses of the best-fit stress model obtained for segment H9, the projections of the slab plane, and the primary and auxiliary planes of the best-fit stress model.

Lower WBZ volume

The data in the lower WBZ subvolume beneath Hokkaido show T axes that are strike aligned and cluster toward north, the P axes show a girdle pattern in a plane normal to the slab plane (Fig. 5b). This pattern is similar to the observed one in H9, but here the T axes are steeper than those in H9. The results form the stress inversion show homogeneous stress field characterized by strike aligned $\sigma 3$ dipping north at about 50°, and $\sigma 1$ of SE trend being strike normal beneath the southern part of the island and slab normal beneath its northern part (Fig. 5b, Table 2). The strike aligned $\sigma 3$ indicates for lateral stretching of the lower WBZ subvolume. A characteristic feature here is that the direction of $\sigma 3$ for both considered subvolumes H7–8 and H10–11 is resolved better than the direction of the maximum compression

σ1 (note the griddle pattern of the 95% confidence limits for σ1, Fig., 5b). We found two models of similar misfits for segments H10–11 having similar directions of σ3 (see Table 2) but different orientations of σ1 - SE and SW, respectively. The above indicates some instability in the orientation of the maximum compression in the lower H10–11 WBZ subvolume. Another specific feature is the similar orientation of σ3 with that in segment H9, i.e. in the DZ. The close to in slab σ3 and σ2, the close to slab normal σ3 and the values of R indicate that the stress regime in all the lower WBZ subvolumes is of general extension (Guiraud *et al.,* 1989).

5. Conclusions

The results of this study clearly indicate 3-planar distribution of stresses in the Wadati-Benioff zone beneath North Honshu and the Hokkaido corner. The stress field in Plane 1 (low-angle thrust faults) is characterized by shallow dipping and close to strike normal maximum compression σ1, the minimum compression σ3 is down dipping. The directions of the best-fit stress models here indicates that the preferred faulting occurs on planes that almost coincide with the slab and slip vectors being slab parallel. Plane 2 (the upper surface of the WBZ below 60〜70 km) is under slab parallel σ1 and close to slab normal σ3 with the exception of the Hokkaido corner where σ3 rotates counterclockwise at about 30° relatively to the slab normal. Plane 3 (the lower surface of the WBZ) is characterized by close to slab normal σ1 and close to slab parallel σ3. The stress regime in Plane 1 and Plane 2 is of general compression with the Hokkaido corner (segment HT) being an exception - Plane 1 is under general extension here. The stress regime in Plane 3 (the lower surface of the WBZ) is of pure extension.

We outlined two subvolumes (upper and lower) in the WBZ beneath Hokkaido, characterized by different orientations of the principle stresses. The stress field in the upper WBZ subvolume is perturbed by a deformation zone, located beneath central Hokkaido (segment H9), perpendicular to the slab's strike and cutting through the slab. The stresses in the upper and lower WBZ subvolumes in this deformation zone are of similar orientation. The directions of the best-fit stress model here suggest that the preferred faulting occurs on an almost vertical plane, the northern wall of which moves down while it's southern wall moves up (see Fig. 6). We suppose that the DZ might represent a crack or a tear cutting through the entire slab (both the upper and lower WBZ subvolumes). Another plausible explanation for the observed stress field in DZ is deformations related to slab contortion without tearing of the slab. The orientation of σ3 in the lower WBZ subvolume beneath HI is similar to that in the DZ and indicates that north trending lateral stretching is not a local phenomenon for the DZ but takes place in the whole lower part of the slab. Possible reasons for a lateral stretching can be the hinge folding of the slab localised in the area of segment H8 and partially in H7 (Moriya, 1978) and/or the increase of the slab's dip beneath central Hokkaido (Katsumata *et al.,* 2003). It should be noted that the location of the identified in the present study DZ approximately coincides with the Tokachi-Oki slab-cracking zone suggested by Katsumata *et al.* (2003). According to them, the slab-cracking zone is well explained by the rapid increase of the WBZ dip angle beneath central Hokkaido, the analysis of 33 FMS for earthquakes located on the upper surface of the WBZ, and on an unusual clustering of micro earthquakes found out in the subduction zone. According to their study, the observed close to trench-parallel orientations of the T axes of 13 earthquake FMS in the transition zone (see A2 in Fig.2) indicate for extensional stresses related to the rapid change in the subduction angle. Our results, obtained by different approach allowing quantitative estimate of the stress field parameters, and by the use of FMS data covering a longer time period, support their interpretation and indicate that strike-aligned extension is dominant not only in the DZ but also in the lower WBZ subvolume. Whether or not the identified here DZ represents a slab-tear can be clarified by further studies on the detail structure of the WBZ beneath central Hokkaido (e.g. velocity structure by active and passive seismic sources).

We present here newly obtained results from studying stresses field in the Pacific Plate subducting beneath North Honshu, the Hokkaido corner and Hokkaido Island. The results can be discussed further to constrain the contemporary dynamics of the subduction process at the Japan-Kurile arc-arc junction, which is beyond the scope of the present study.

Acknowledgements

The authors thank John Gephart for providing the latest version of the FMSI software package. CCH is grateful to Velko Hristov for helping with the data format, to Christopher Scholz for helpful discussion and to an anonymous reviewer for constructive comments and suggestions. The research was conducted during CCH's stay at ERI in 2006 under the program of the International Earthquake and Volcano Research Promotion by ERI, the University of Tokyo.

References

Angelier, J., 1998. A new direct inversion of earthquake focal mechanisms to reconstruct the stress tensor. (abstract). Ann. Geophys. Part I, Suppl. I to v.16, C115 XXIII Gen. Assembly of EGS, 20–24 April 1998, Nice, France.

Caccamo, D., Neri, G., Sarao, A. and Wyss, M., 1996. Estimates of stress directions by inversion of earthquake fault-plane solutions in Sicily. *Geophys. J. Int.* **125**, 857–868.

Christova, C., 2001. Depth distribution of stresses in the Kamchatka Wadati-Benioff zone inferred by inversion of earthquake focal mechanisms. *J. Geodynamics* **31**, 355–372.

Christova, C., 2004. Stress field in the Ryukyu-Kyushu Wadati-Benioff zone by inversion of earthquake focal mechanisms. *Tectonophysics* **384**, 175–189.

Christova, C., 2005. Space distribution of the contemporary stress field in the Izu-Bonin Wadati-Benioff zone by inversion of earthquake focal mechanisms. *J. Geodynamics* **39**, 413–428.

Christova C., Nikolova, S.B., 1998. New results on the contemporary plate tectonics in the Aegean region from seismological observations. *Phys. Chemistry of the Earth* 23/7–8, 785–798.

Christova, C., Tsapanos, T., 2000. Depth distribution of stresses in the Hokkaido Wadati-Benioff zone as deduced by inversion of earthquake focal mechanisms. *J. Geodynamics* **30**, 557–573.

Christova, C. and Scholz, C.H., 2003. Stresses in the Vanuatu subducting slab: A test of two hypotheses. *Geophys. Res. Lett.* **30**, 15, 1790–1793.

DeMets, C., Gordon, R.G., Argus, D.F. and Stein, S., 1994. Effect of recent revisions to the geomagnetic reversal time scale on estimates of current plate motions, *Geophys. Res. Lett.,* **21**, 2191–2194.

Frohlich, C. and Davis, S.D., 1999. How well constrained are well-constrained T, B and P axes in moment tensor catalogues? *J. Geophys. Res.* **104**, 4901–4910.

Gephart, J. and Forsyth, D., 1984. An improved method for determining the regional stress tensor using earthquake focal mechanism data: application to the San Fernando earthquake sequence. *J. Geophys. Res.* **89**, 9305–9320.

Gillard, D., M.Wyss, Okubo, P., 1996. Type of faulting and orientation of stress and strain as a function of space and time in Kilauea's south flank, Hawaii. *J. Geophys. Res.* **101**, 16025–16042.

Guiraud, M., Laborde, O., Philip, H., 1989. Characterization of various types of deformation and their corresponding deviatoric stress tensors using microfault analysis. *Tectonophysics* **170**, 289–316.

Hasegawa, A., Umino, N. and Takagi, A., 1978. Double-planed structure of the deep seismic zone in the northeastern Japan arc. *Tectonophysics* **47**, 43–58.

Hasegawa, A., Umino, N., Takagi, A., Suzuki, S., Motoya, Y., Kameya, S., Tanaka, K. and Sawada, Y., 1983. Spatial distribution of earthquakes beneath Hokkaido and Northern Honshu, Japan. *J. Seismol Soc. Jpn.* **36**, 129–150 (in Japanese with English abstract).

Helfrich, G.R., 1997. How good are routinely determined focal mechanisms? Empirical statistics based on a comparison of Harvard. USGS and ERI moment tensors, *Geophys. J. Int.* **131**, 741–750.

Igarashi, T., T. Matsuzawa, N. Umino and A. Hasegawa, 2001. Spatial distribution of focal mechanisms for interplate and intraplate earthquakes associated with the subducting Pacific plate beneath the northeastern Japan arc: A triple-planed deep seismic zone, *J. Geophys. Res.* **106**, 2177–2191.

Isacks, B.L.and Molnar, P., 1971. Distribution of stresses in the descending lithosphere from a global survey of focal mechanism solution of mantle earthquakes. *Rev. Geophys.* **9**, 103.

Japan Meteorological Agency. The Annual Seismological Bulletin of Japan (1997, 1998, 1999, 2000, 2001, 2002, 2003, 2004), (CD-ROM).

Japan Meteorological Agency, 2005. The Seismological and Volcanological Bulletin for January - December 2005 (CDC-ROM).

Katsumata K., Wada N. and Kasahara M., 2003. Newly imaged shape of the deep seismic zone within the subducting Pacific plate beneath the Hokkaido corner, Japan-Kurile arc-arc junction. *J. Geophys. Res.* **108** (B12), 2565, doi: 10.1029/2002JB002175.

Kosuga, M., Sato, T., Hasegawa, A., Matsuzawa, T., Suzuki, S. and Motoya, Y., 1996. Spatial distribution of intermediate-depth earthquakes with horizontal or vertical nodal planes beneath northeastern Japan. *Phys. Earth. Planet. Int.* **93**, 63–89.

Lu, Z., Wyss, M. and Pulpan, H., 1997. Details of stress directions in the Alaska subduction zone from fault plane solutions. *J. Geophys. Res.* **102**, 5385–5402.

McKenzie, D.P., 1969. The relation between fault plane solutions for earthquakes and the directions of principle stresses. *Bull. Seismol. Soc. Am.* **59**, 591–601.

Michael, A.J., 1984. Determination of stress from slip data: faults and folds. *J. Geophys. Res.* **89**, 11517–11526.

Miller, M.S., Kennet, B.L.N. and Gorbatov, A., 2006. Morphology of the distorted subducted Pacific slab beneath the Hokkaido corner, Japan. *Phys. Earth Planet. Int.* **156**, 1–11.

Moriya, T., 1978. Seismic studies of the upper mantle beneath the arc-junction at Hokkaido: folded structure of intermediate depth seismic zone and attenuation of seismic waves. *J. Phys. Earth* **26**, S467–S475.

Parker, R. and McNutt, M., 1980. Statistics for the one-norm misft measure. *J. Geophys. Res.* **85**, 4429–4430.

Sasatani, T., 1976. Mechanisms of mantle earthquakes near the junction of the Kurile and northeastern Honshu arcs. *J. Phys. Earth.* **24**, 341–353.

Seno, T. and Pongsawat, B., 1981. A triple-planed structure of seismicity and earthquake mechanisms at the subduction zone off MIYagi Prefecture, northern Honshu, Japan. *Earth. Planet. Int.* **55**, 25–36.

Stauder, W. and Mualchin, L., 1976. Fault motion in the larger earthquakes of the Kurile-Kamchatka Arc and of the Kurile-Hokkaido corner. *J. Geophys. Res.* **81**, 297–308.

Suzuki, S., Sasatani, T. and Motoya, Y., 1983. Double seismic zone beneath the middle of Hokkaido, Japan, in the sowthwestern side of the Kurile arc. *Tectonophysics* **96**, 59–76.

Takahashi, H., Kasahara, M., Kimata, F., Miura, S., Heki, K., Seno, T., Kato, T., Vasilenko, N., Ivaschenko, A., Bahtiarov, V., Levin, V., Gordeev, E., Korchagin, F. and Gerasimenko, M., 1999. Velocity field of around the Sea of Okhotsk and Sea of Japan regions determined from new continuous GPS network data. *Geophys. Res. Lett.,* **26**, 2533–2536.

Umino, N., Hasegawa, A., 1975. On the two-layered structure of deep seismic plane in northeastern Japan arc. Japan, *J. Seismol. Soc. Jpn,* **27**, 125–139 (in Japanese with English abstract).

Umino, N., Hasegawa, A., Takagi, A., Suzuki, S., Motoya Y., Kameya, S., Tanaka, K. and Sawada, Y., 1984. Focal Mechanisms of intermediate-depth earthquakes beneath Hokkaido and Northern Honsu, Japan, *J. Seismol. Soc. Jpn,* **37**, 523–538 (in Japanese with English abstract).

Yoshii, T., 1979, A detailed crosssection of the deep seismic zone beneath northeastern Honshu, Japan. *Tectonophysics* **55**, 349–360.

(Received July 31, 2006)
(Accepted December 11, 2006)